Engineering Science and Technology, an International Journal 19 (2016) 538–547

HOSTED BY

Contents lists available at ScienceDirect

Engineering Science and Technology, an International Journal

journal homepage: http://www.elsevier.com/locate/jestch

Full Length Article

# Numerical study of unsteady blood flow through a vessel using Sisko model

Akbar Zaman [a,*], Nasir Ali [a], O. Anwar Bég [b]

[a] Department of Mathematics and Statistics, International Islamic University, Islamabad, 44000, Pakistan
[b] Gort Engovation (Propulsion and Biomechanics) Research, Gabriel's Wing House, 15 South mere Avenue, Bradford, UK

ARTICLE INFO

*Article history:*
Received 5 June 2015
Received in revised form
3 September 2015
Accepted 16 September 2015
Available online 27 October 2015

*Keywords:*
Unsteady pulsatile flow
Blood
Sisko fluid
Body acceleration
Finite difference method

ABSTRACT

A mathematical study for two-phase unsteady pulsatile flow of blood through a vessel in the presence of body acceleration is presented in this paper. The blood in the core region is modeled as a non-Newtonian fluid while in the peripheral region it is described as a Newtonian fluid. The effects of body acceleration are also taken into account in this study. The continuity and momentum equations are used to model the proposed problem in terms of a nonlinear partial differential equation. This equation along with initial and boundary conditions is made dimensionless and then solved numerically using finite difference method. The behavior of various flow quantitates is analyzed through a parametric study.



## 1. Introduction

Blood composition consists of aqueous plasma, red blood cells (RBCs, 98% by volume), some white blood cells (WBCs), and platelets and a variety of lipoproteins [1]. Plasma particles consist of various proteins, including clotting factors (fibrinogen) and various ions. Although red blood cells are very numerous and morphologically very simple, they contain hemoglobin, which transports oxygen throughout the body. The rheological features of blood are characterized by its components and their interactions with each other. Blood shows anomalous behavior while flowing through a large vessel (femoral artery) because its viscosity varies along the diameter of the vessel which depicts Fahraeus–Lindqvist (F-L) effect. The definition of F-L effect is given in the literature as a phenomenon in which the viscosity of a fluid/blood changes with the diameter of the vessel. This effect is observed due to migration of suspended cells in the radial direction which is due to variation of composition of blood [2–4]. In order to capture the F-L effect, the blood flow in arteries is treated as two-phase. The core layer is treated as a non-Newtonian while peripheral layer is modeled as a Newtonian fluid. Since the flow of blood in arteries is generated by pulsatile pressure gradient produced by the pumping action of the heart, several authors examined the F-L effects by considering the flow to be unsteady. For instance, Majhi and Usha [5] have examined the F-L effect by considering third grade non-Newtonian fluid in the core. In another study, Majhi and Nair [6] followed the same study in the presence of body acceleration. Haldar and Andersson [7] investigated the two-layer blood flow in a cosine shape artery considering Casson model for blood. The pulsatile flow of blood in the presence of body acceleration was examined by Usha and Prema [8] by considering blood as Newtonian fluid.

The non-Newtonian properties exhibited by blood like shear-thinning at high shear rate [9–11] and visco-elasticity at low shear rate [12,13] motivated several other researchers to incorporate different non-Newtonian model while analyzing blood flow problems. In this regard, single-layer pulsatile flow of blood using different non-Newtonian fluid models can be found in the literature. [14–19]. Recently, two-layer pulsatile flow of blood with body acceleration using a generalized second grade fluid model was investigated by Massoudi and Phuoc [20]. In another study, Sankar [21] used Herschel–Bulkley fluid in the core to discuss the pulsatile two-layer flow of blood. The unsteady pulsatile flow problems in context of dusty fluid were recently analyzed by Madhura et al. [22] and Gireesha et al. [23,24].

In the present study we are interested to extend the idea of Massoudi and Phuoc [20] by considering the Sisko model in the core. It is noted from the study carried out by Massoudi and Phuoc that the material parameters of the modified second grade fluid model do not appear in the governing equation of the flow. In fact for the particular flow situation considered by Massoudi and Phuoc the modified second grade model and power-law model yield the same

* Corresponding author. Tel.: +92 519019756.
*E-mail address:* akbarzaman75@yahoo.com (A. Zaman).
Peer review under responsibility of Karabuk University.

http://dx.doi.org/10.1016/j.jestch.2015.09.013

governing equation. The Sisko model used here is a generalization of the power-law model. In this way our analysis is general and include the results of Massoudi and Phuoc as a special case. Moreover, under pulsatile flow conditions, the blood is exposed to high/low and medium shear rates in a single cardiac cycle. Branes et al. [25] have showed that power law model most suitably captures the blood rheology at medium shear rates, but it is not suitable for high/low shear rates. In such situation, the Sisko model is the most appropriate choice to depict the blood properties at high shear as compared to other non-Newtonian models. The article is organized in the following fashion: Fundamental equations and mathematical formulation is described in detail in sections 2 and 3. Finite difference method is evaluated for the developed nonlinear system of equations. The details are given in sections 4 and 5. Section 6 comprises results and their discussion under the influence of various parameters of interest. Finally, some concluding remarks are drawn in section 7.

## 2. Fundamental equations

Flow equations for an incompressible fluid are given by

$$\nabla \cdot \boldsymbol{u} = 0, \tag{1}$$

$$\rho \frac{d\boldsymbol{u}}{dt} = \nabla \cdot \boldsymbol{T} + \rho G(t), \tag{2}$$

where $\boldsymbol{u}$ is the fluid velocity, $\rho$ is the density, $\boldsymbol{T}$ is the Cauchy stress tensor and $d/dt$ is the material time derivative given by:

$$\frac{d(\cdot)}{dt} = \frac{\partial(\cdot)}{\partial t} + (\boldsymbol{u} \cdot \nabla). \tag{3}$$

The Cauchy stress tensor for a Sisko fluid is given by Reference 26:

$$\boldsymbol{T} = -p\boldsymbol{I} + \boldsymbol{S}, \tag{4}$$

in which $p$ is the pressure, $\boldsymbol{I}$ is the identity tensor and $\boldsymbol{S}$ is the extra stress tensor defined by

$$\boldsymbol{S} = \left[\varepsilon_1 + \varepsilon_2 \left|\sqrt{\Pi}\right|^{n-1}\right] \boldsymbol{A}_1^*, \tag{5}$$

where $n$, $\varepsilon_1$ and $\varepsilon_2$ are the material parameters defined differently for different fluids. Note that for $n = 1$ or $\varepsilon_2 = 0$, the Newtonian fluid model is recovered and if $\varepsilon_1 = 0$ then the generalized power law model can be obtained. $\boldsymbol{A}_1^*$ is the first Rivlin-Ericksen tensor defined by

$$\boldsymbol{A}_1^* = \boldsymbol{L} + \boldsymbol{L}^T \tag{6}$$

$$\text{in which} \quad \boldsymbol{L} = \nabla \boldsymbol{u}, \tag{7}$$

$$\text{and} \quad \Pi = \frac{1}{2}\text{tr}(\boldsymbol{A}_1^{*2}). \tag{8}$$

## 3. Mathematical formulation

For the present analysis, the artery is assumed to be a circular tube. For mathematical formulation, we have employed the cylindrical co-ordinates $(r, \theta, z)$ system. Following Reference 27, a local acceleration term is also included in the momentum equation. The geometry of the flow configuration is presented in Fig. 1.

It can be shown that the radial velocity is negligibly small in magnitude and may be neglected for low Reynolds number flow. For the present case the velocity field is taken as

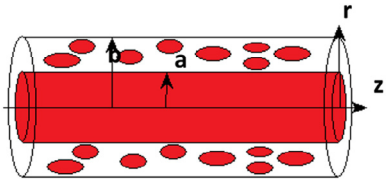


**Fig. 1.** Schematic diagram of flow in vessel.

$$\boldsymbol{u}_i = [0, 0, u_i(r,t)], i = 1, 2. \tag{9}$$

Using Eq. (9), continuity equation is identically satisfied and z-component of equation of motion gives

$$\rho \frac{\partial u_i}{\partial t} = -\frac{\partial p}{\partial z} + \rho G(t) + \frac{1}{r}\frac{\partial}{\partial r}(rS_{rz}), i = 1, 2. \tag{10}$$

We have divided our domain $0 \le r \le b$ as $0 \le r \le a$ (a core region) and $a \le r \le b$ (a periphery region). It is also assumed that the fluid in the core is a Sisko fluid [26] and in the periphery a Newtonian fluid. Thus the shear stress tensor is given by

$$S_{rz} = \begin{cases} \left[\varepsilon_1 + \varepsilon_2 \left|\dfrac{\partial u_1}{\partial r}\right|^{n-1}\right]\left(\dfrac{\partial u_1}{\partial r}\right), & 0 \le r \le a, \\ \mu \dfrac{\partial u_2}{\partial r}, & a \le r \le b, \end{cases} \tag{11}$$

Where $\mu$ is the viscosity of the Newtonian fluid and the equation for pressure gradient is taken from Reference 28:

$$-\frac{\partial p}{\partial z} = A_0 + A_1 \cos \omega_p t, \tag{12}$$

where $\partial p/\partial z$ is the pressure gradient produced by the pumping action of the heart, $A_0$ is the systolic component of the pressure gradient, $A_1$ is the amplitude (diastolic) of the fluctuation of the pressure gradient, $\omega_p = 2\pi f_p$ is the circular frequency and $f_p$ is the pulse rate frequency. Further, the body acceleration is given by References 6, 20, 29, and 30.

$$G(t) = A_g \cos(\omega_b t + \phi), \tag{13}$$

where $A_g$ is the amplitude, $f_b$ is the frequency [$\omega_b = 2\pi f_b$] and $\phi$ is the lead angle of $G$ with respect to the heart action. Eliminating $S_{rz}$ between (10) and (11), the equation in the core region is obtained as, i.e. $0 \le r \le a$

$$\rho \frac{\partial u_1}{\partial t} = A_0\left(1 + \frac{A_1}{A_0}\cos(\omega_p t)\right) + \rho A_g \cos(\omega_b t + \phi) + \frac{1}{r}\frac{\partial}{\partial r}\left\{r\left[\varepsilon_1 + \varepsilon_2\left|\left(\frac{\partial u_1}{\partial r}\right)^{n-1}\right|\right]\left(\frac{\partial u_1}{\partial r}\right)\right\}. \tag{14}$$

Similarly, for the periphery region, i.e. $a \le r \le b$,

$$\rho \frac{\partial u_2}{\partial t} = A_0\left(1 + \frac{A_1}{A_0}\cos(\omega_p t)\right) + \rho A_g \cos(\omega_b t + \phi) + \frac{\mu}{r}\frac{\partial u_2}{\partial r} + \mu \frac{\partial^2 u_2}{\partial r^2}. \tag{15}$$

The boundary and initial conditions for the present flow configuration are

$$\left.\frac{\partial u_1(r,t)}{\partial r}\right|_{r=0} = 0, (\text{Symmetry condition})$$

$$u_2(r,t)|_{r=b} = 0, (\text{No-slip condition})$$

$$u_1(r,t)|_a = u_2(r,t)|_a,$$
$$\left[\varepsilon_1+\varepsilon_2\left|\left(\frac{\partial u_1}{\partial r}\right)^{n-1}\right]\left(\frac{\partial u_1}{\partial r}\right)\right|_{r=a} = \mu\left.\frac{\partial u_2}{\partial r}\right|_{r=a},$$

$$u_1(r,t)=u_2(r,t)=0, \quad at\ t=0. \quad \text{(Initial conditions)} \tag{16}$$

The last two boundary conditions in Eq. (16) represent the continuity of velocities and stresses at the interface. The flow rate and shear stress at wall are respectively given by

$$Q=\int_0^a u_1 r dr+\int_a^b u_2 r dr, \tag{17}$$

$$\tau_s=-\mu\left(\frac{\partial u_2}{\partial r}\right)_{r=b}. \tag{18}$$

## 4. Dimensionless formulation of the problem

Introducing the dimensionless variables [20]

$$\bar{r}=\frac{r}{b}, \bar{u}=\frac{u}{U_0}, \bar{t}=\frac{\omega_p}{2\pi}t, \tag{19}$$

Eqs. (14) and (15) may be cast as (after dropping bars)

$$\begin{aligned}\alpha\left[\frac{\partial u_1}{\partial t}\right] &= B_1(1+e\cos(2\pi t))+B_2(\cos(2\pi\omega_r t+\phi))\\ &+\frac{1}{r}\left\{\left[\varepsilon+\left|\left(\frac{\partial u_1}{\partial r}\right)^{n-1}\right]\left(\frac{\partial u_1}{\partial r}\right)\right\}+\\ &+\left\{\left[\varepsilon+\left|\left(\frac{\partial u_1}{\partial r}\right)^{n-1}\right]\frac{\partial^2 u_1}{\partial r^2}\right\}+\left(\frac{\partial u_1}{\partial r}\right)\left\{\frac{\partial}{\partial r}\left(\left|\left(\frac{\partial u_1}{\partial r}\right)^{n-1}\right|\right)\right\},\end{aligned} \tag{20}$$

$$\gamma\frac{\partial u_2}{\partial t}=\hat{B}_1(1+e\cos(2\pi t))+\hat{B}_2(\cos(2\pi\omega_r t+\phi))+\frac{1}{r}\left[\frac{\partial u_2}{\partial r}\right]+\frac{\partial^2 u_2}{\partial r^2}. \tag{21}$$

The dimensionless boundary conditions become

$$\left.\frac{\partial u_1}{\partial r}\right|_{r=0}=0, \text{(Symmetry)}$$

$$u_2|_{r=1}=0, \text{(No-slip condition)}$$

$$u_1|_{r_0}=u_2|_{r_0},$$
$$\left[\varepsilon+\left|\left(\frac{\partial u_1}{\partial r}\right)^{n-1}\right]\left(\frac{\partial u_1}{\partial r}\right)\right|_{r=r_0}=\mu^*\left.\frac{\partial u_2}{\partial r}\right|_{r=r_0}. \quad \text{(At interface of the radius)} \tag{22}$$

It is pointed out that Eq. (20) reduces to the corresponding equation of Massoudi and Phuoc [20] when $\varepsilon\to 0$. The volume flow rate and the shear stress at wall are respectively given by

$$Q=\left(\int_0^{r_0} u_1 r dr+\int_{r_0}^1 u_2 r dr\right), \tag{23}$$

$$\tau_s=\left(\frac{\partial u_2}{\partial r}\right)_{r=1}. \tag{24}$$

in which

$$U_0=\left(\frac{A_0 b^2}{\mu}\right), \omega_r=\frac{\omega_b}{\omega_p}, r_0=\frac{b}{a}, \rho^*=\frac{\rho_2}{\rho_1}, \mu^*=\frac{\mu_2}{\bar{\varepsilon}}, \bar{\varepsilon}=\varepsilon_2\left(\frac{U_0}{b}\right)^{n-1},$$
$$\varepsilon=\frac{\varepsilon_1}{\bar{\varepsilon}}, e=\frac{A_1}{A_0}$$

$$B_1=\frac{A_0 b^2}{\bar{\varepsilon}U_0}, B_2=\rho_1 A_g\frac{b^2}{\bar{\varepsilon}U_0}=\frac{\rho_1 A_g}{A_0}B_1, \alpha=\frac{\rho_1\omega_p b^2}{2\pi\bar{\varepsilon}},$$
$$\gamma=\frac{\rho_2\omega_p b^2}{2\pi\bar{\varepsilon}\mu^*}=\frac{\rho_1\omega_p b^2}{2\pi\mu^*}\frac{\rho_2}{\rho_1}=\alpha\frac{\rho^*}{\mu^*},$$

$$\hat{B}_1=\frac{A_0 b^2}{\bar{\varepsilon}U_0\mu^*}=\frac{B_1}{\mu^*}; \hat{B}_2=\frac{\rho_2 A_g b^2}{\bar{\varepsilon}U_0\mu^*}=\rho_1 A_g\frac{b^2}{\bar{\varepsilon}U_0}\frac{\rho_2}{\rho_1\mu^*}=B_2\frac{\rho^*}{\mu^*}. \tag{25}$$

## 5. Numerical solution

We have integrated Eqs. (20) and (21) subject to the boundary and initial conditions given in Eq. (22) numerically by using a finite difference method which is forward in time and central in space. For details about this method see References 19, 31, and 32. Let us denote $u_1(r_i,t_j)$ as $u_{1i}^j$ and approximate various partial derivatives as

$$\frac{\partial u_1}{\partial r}\cong\frac{u_{1i+1}^j-u_{1i-1}^j}{2\Delta r}=u_{1r},$$

$$\frac{\partial^2 u_1}{\partial r^2}\cong\frac{u_{1i+1}^j-2u_{1i}^j+u_{1i-1}^j}{(\Delta r)^2}=u_{1_r{}^2},$$

$$\frac{\partial}{\partial r}\left(\left|\frac{\partial u_1}{\partial r}\right|^{n-1}\right)\cong\frac{\left(\left|\frac{u_{1i+1}^j-u_{1i-1}^j}{2\Delta r}\right|^{n-1}\right)_{i+1}^j-\left(\left|\frac{u_{1i+1}^j-u_{1i-1}^j}{2\Delta r}\right|^{n-1}\right)_{i-1}^j}{2\Delta r}=abs(u_{1r}), \tag{26}$$

Similarly, for the time derivative we define the approximation:

$$\frac{\partial u_1}{\partial t}\cong\frac{u_{1i}^{j+1}-u_{1i}^j}{t}=u_{1t}. \tag{27}$$

Using Eqs. (26) and (27), Eqs. (20) and (21) may be transformed to the following difference equation

$$u_{1i}^{k+1}=u_{1i}^k+\frac{\Delta t}{\alpha}\left[\begin{array}{l}B_1(1+e\cos(2\pi t^k))+B_2(\cos(2\pi\omega_r t^k+\phi))+\\ \left\{\left(\varepsilon+|u_{1r}|^{n-1}\right)u_{1_r{}^2}+(u_{1r})abs(u_{1r})+\frac{1}{r}\left(\varepsilon+|u_{1r}|^{n-1}\right)u_{1r}\right\}\end{array}\right], \tag{28}$$

$$u_{2i}^{k+1}=u_{2i}^k+\left(\frac{t}{\gamma}\right)\left[\begin{array}{l}\hat{B}_1(1+e\cos(2\pi t^k))+\hat{B}_2(\cos(2\pi\omega_r t^k+\phi))\\ +\frac{1}{r}[u_{2r}]+u_{2_r{}^2}\end{array}\right]. \tag{29}$$

For the solution of the present problem we have discretized the radius by using the formula $r_i=(i-1)\Delta r$, $(i=1,2,\ldots.,N_c+1)$ such that $r_{(N+1)}=r_{core}$ and $r_i=(i-(N_c+1)), i=(N_c+1,N_c+2,\ldots\ldots,N+1)$ with the following central difference approximation $r_{N+1}=1$, where $\Delta r$ is the increment in the radial direction. Similarly for discretization of time, we have used the following discretization formula $t_j=(j-1)\Delta t, (i=1,2,\ldots..)$, where $\Delta t$ is the small time increment. We have considered the following step size $\Delta r=0.025$ and the time step as 0.00001 for the present problem, so that the results may converge to the accuracy of an order $\sim 10^{-7}$.

## 6. Graphical results and discussion

To observe the quantitative effects of the Sisko material parameter, computer code is developed for the numerical simulations in Matlab. In this study, generally we have taken $\varphi=0$ and the radius of the core is to be 60% of the radius of the tube. Our results are based on the data of two different arteries (radius): for smaller vessel,

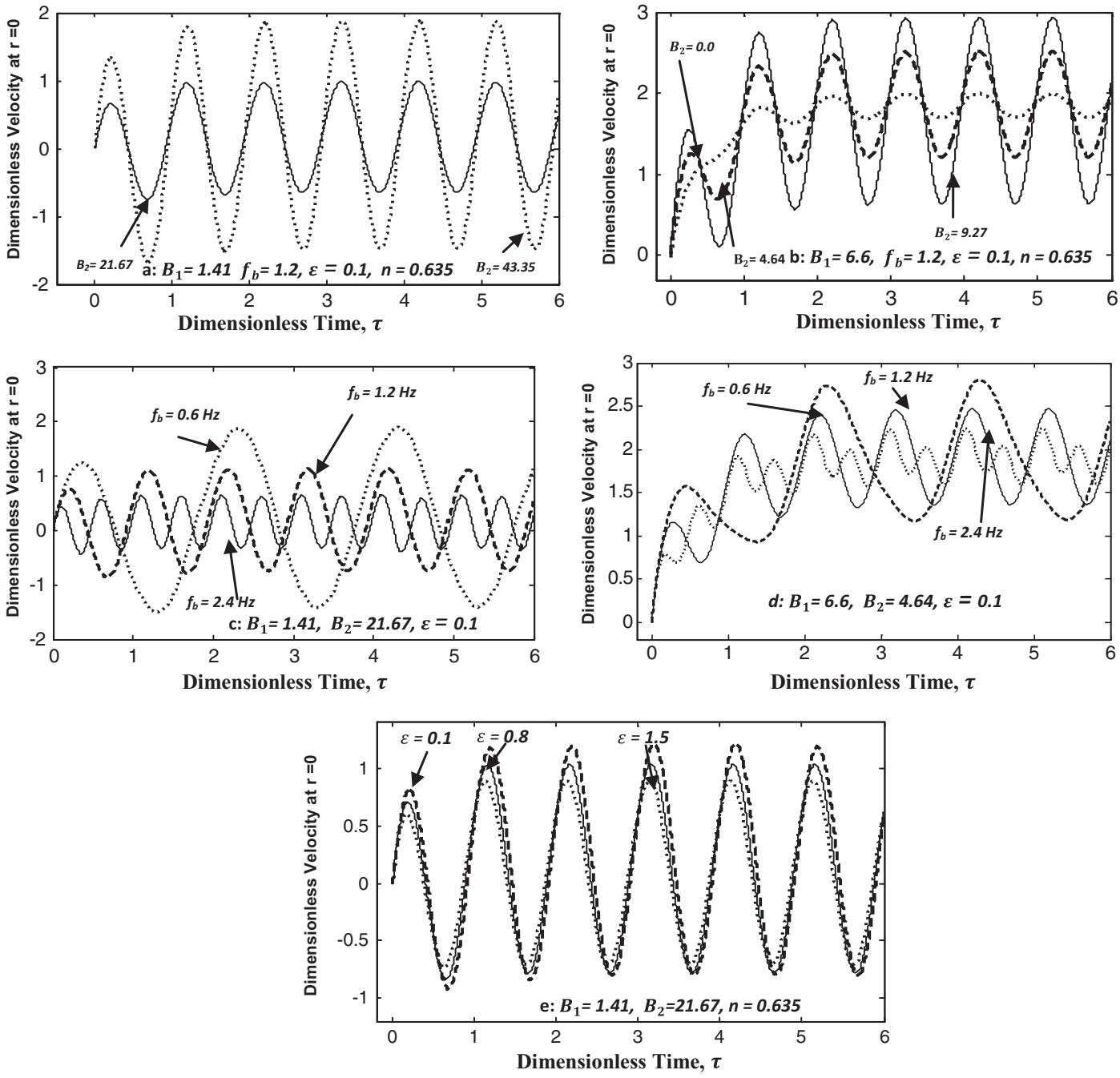


**Fig. 2.** Time-series of velocity at r = 0 for flow in two arteries, where (a), (c) and (e) are for larger artery (r = 0.5 cm, $A_0$ = 32 dyne/cm$^3$) and (b) and (d) are for smaller artery (r = 0.15 cm, $A_0$ = 698.65 dyne/cm$^3$). Velocity graphs for different values of $B_2$ (varying $A_g$) are shown in (a), (b); velocity graphs for different values of $f_b$ are shown in (c) and (d); velocity graphs for different values of $\varepsilon$ are shown in (e).

coronary artery, the data are chosen as ( $A = 698.65\, dyne/cm^3$, $r = 0.15\, cm$ ) and for larger vessel, femoral artery, the data are chosen as ( $A = 32\, dyne/cm^3$, $r = 0.5\, cm$ ) [18] and value of *Womersley number* is chosen as 2.

The time-series of velocity at the central plane are shown in Fig. 2 for both femoral and coronary arteries. These graphs show that irrespective of the artery type, the velocity at the center fluctuates around its mean value, increases and finally reaches the steady state condition as the time increases (here we define $\tau_s$ is the dimensionless steady state time where the maximum velocity distribution is obtained). Fig. 2(a) and (b) shows that the amplitude of the velocity increases by increasing the amplitude of the body acceleration while it shows decreasing trend by increasing the pulse frequency $f_b$ (Fig. 2c,d) and material parameter of the Sisko model (Fig. 2e).

A comparison of our numerical results in the limiting case when $\varepsilon \to 0$ with that of Massoudi and Phuoc [20] is presented in Fig. 3. Here radial and time evolutions of axial velocity for coronary artery are compared. It is observed that our results are in pleasing agreement with the existing results of Massoudi and Phuoc [20]. This obviously corroborates the validity of our model and further strengthens our faith on results obtained through it.

The velocity profiles at different time instances for femoral artery are shown in Fig. 4. It is generally observed from these plots that the body acceleration increases the magnitude of velocity while an

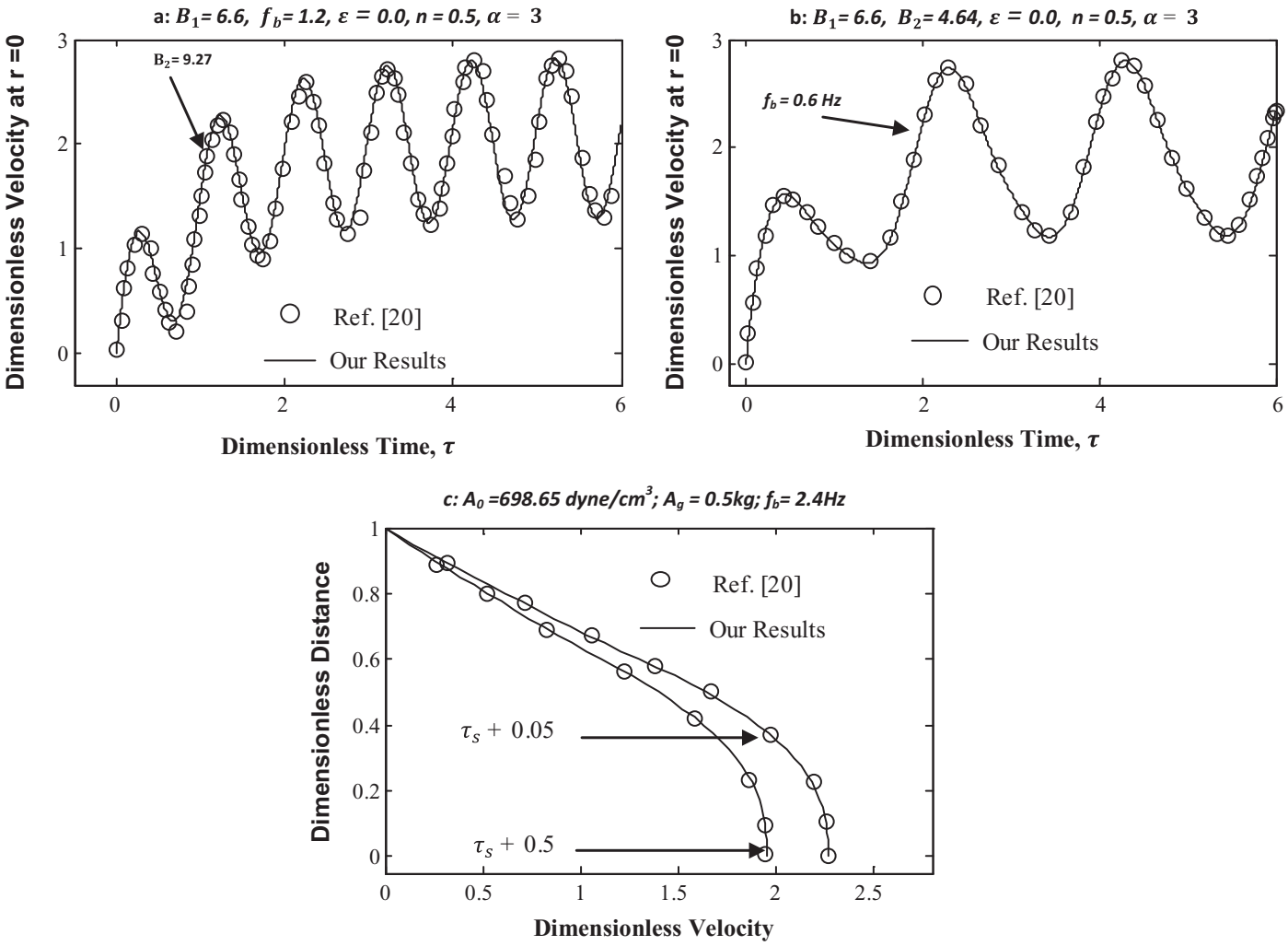


**Fig. 3.** Comparison graphs of finite difference method with Massoudi and Phuoc results for coronary artery.

increase in pulse frequency $f_b$ decreases its magnitude. There are inflection points within the time cycle of the velocity profile where the shapes of velocity changes from convex to concave. It is observed from Fig. 4(a) that the shape of the velocity profile is parabolic in the absence of body acceleration at the beginning of the fluctuation cycle or $t = t_s$ as evident in Fig. 4(b). Fig. 4(c) and (d) indicates that the maximum velocity shifts from the center of an artery toward the wall during the first half of fluctuation cycle and then moves back to the center of an artery during the second half of fluctuation cycle. The core region is taken as Newtonian and the effects of body acceleration are minimized in comparison with other panels in Fig. 4(e). It is noted from this figure that the velocity profile returns to its parabolic shape and the curve becomes concave at $t = t_s + t_{half}$. In Fig. 4(f) the core region is assumed as non-Newtonian fluid and the effect of body acceleration is increased. This results in the forward shift of the fluctuation cycle.

The velocity profile for smaller artery, coronary artery, is shown in Fig. 5. Fig. 5(a–b) shows that the velocity profiles follow the same pattern as shown in Fig. 4. A comparison of the velocity profiles in Figs. 4 and 5 for two arteries reveals that the velocity is faster in larger artery as compared to smaller artery while its grows significantly slowly for Newtonian case as compared to the non-Newtonian case. Fig. 5(g) shows the effect of material parameter of the Sisko model. It is found that the magnitude of velocity increases by decreasing $\varepsilon$ which ultimately shows that velocity profile is a decreasing function of material parameter. Fig. 5(h) shows a decrease in velocity by increasing the thickness of the peripheral layer.

Figs. 6 and 7 present the effects of body acceleration $A_g$, body force $f_b$, shear-thinning and material parameter on the dimensionless flow rate and the dimensionless shear stress. The profiles indicate that the flow rate and the wall shear stress fluctuate around mean values and these mean values become constant values when steady state conditions are achieved. It is also observed that the amplitude of fluctuation increases with an increase in the amplitude of body acceleration while it shows converse behavior with increasing the material constant of the Sisko model. The fluctuation of these profiles is always between a positive and a negative value in the time cycle for the larger artery, while for the small artery such fluctuations of wall shear stress in the smaller artery are significantly higher (about three to five times) than those obtained for the larger artery.

Now, we would like to comment on the significance of the Sisko model in the light of the above discussion.

It has been pointed by Yilmaz and Gundogdu [1] that all the generalized Newtonian fluid models of (blood) viscosity show shear-thinning behavior and must meet the following requirements. They must effectively fit the viscosity shear rate data of blood at all shear rates, whether high, medium or low. Power-law model is suitable for blood at medium shear rates. However, it does not represent the blood rheology at low and high shear rates. In fact power-law

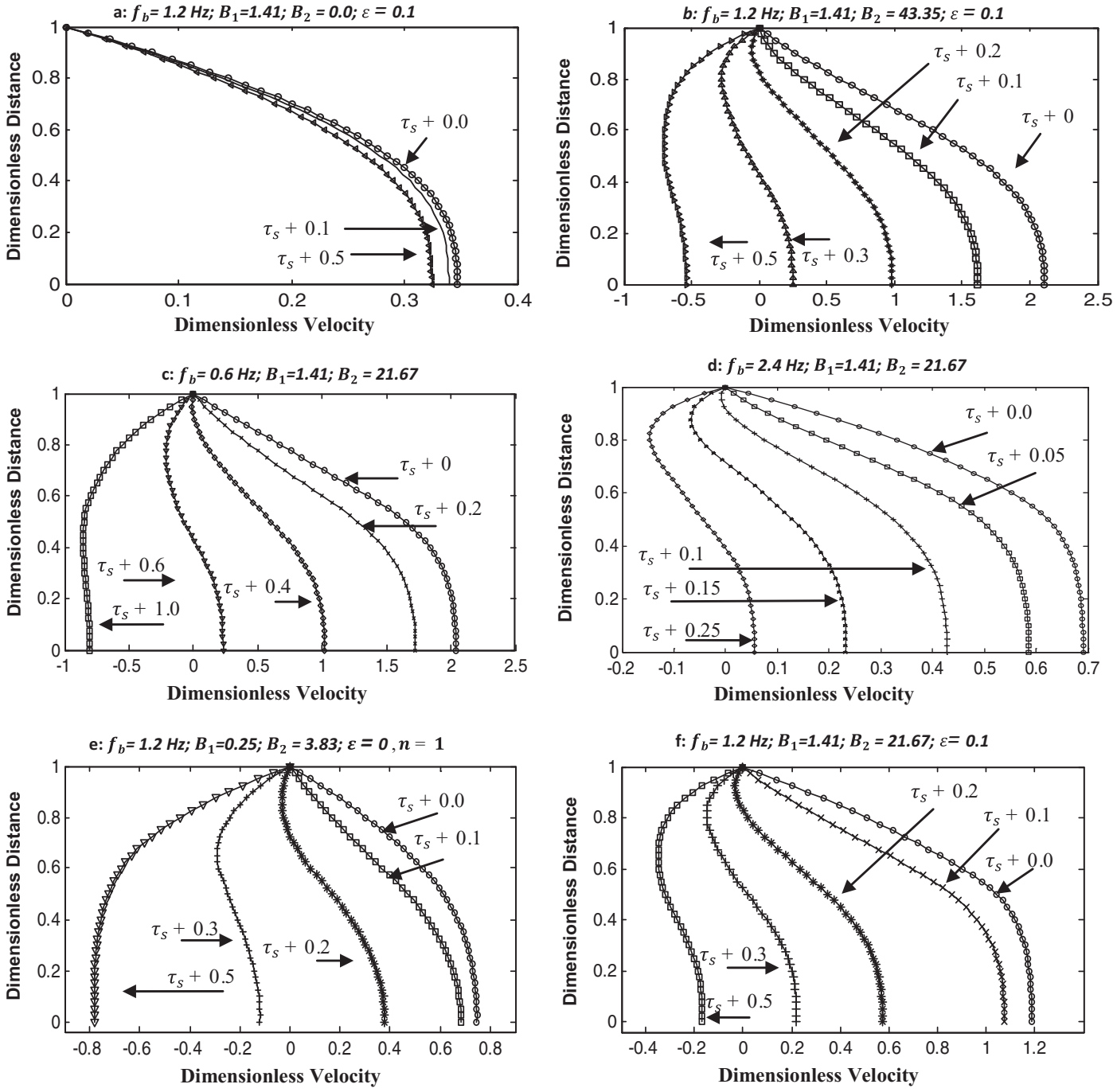


**Fig. 4.** Radial distribution of axial velocity graphs for larger artery (r = 0.5 cm, $A_0$ = 32 dyne/cm$^3$). Velocity graphs for different values of $B_2$ (varying $A_g$) are shown in (a) and (b); graphs for different values of $f_b$ are shown in (c) and (d); graphs for different values of $B_1$ and $B_2$ are shown in (e) and (f).

equation predicts infinite viscosity at low shear rate and zero viscosity as shear rate approaches to infinity. The Sisko model extends the power-law model to include a finite value of viscosity as shear rates approach infinity. In this sense, the Sisko model is better capable of predicting the blood rheology at high shear rates. Graphical illustrations show that the additional constant $\mu_\infty$ ( $\varepsilon$ in dimensionless form) in the Sisko equation significantly alters the flow characteristics of blood. It is observed that the power-law model predicts higher value of the amplitude of dimensionless velocity at $r = 0$ than the Sisko model. Similar is the case with dimensionless radial velocity. This significant effect of $\varepsilon$ on velocity is later transmitted in other variables such as flow rate and wall shear stress. It is found that flow rate through artery decreases while wall shear stress increases in going from power-law to the Sisko model. For instance, keeping the other parameters fixed, a decrease of 20% is noted in the flow rate as $\varepsilon$ changes from 0 to 1.5.

The above discussion clearly shows that inclusion of $\varepsilon$ in the power law equation brings significant qualitative changes in the results.

## 7. Concluding remarks

A mathematical model for two-layer unsteady pulsatile flow in the presence of body acceleration is derived using the

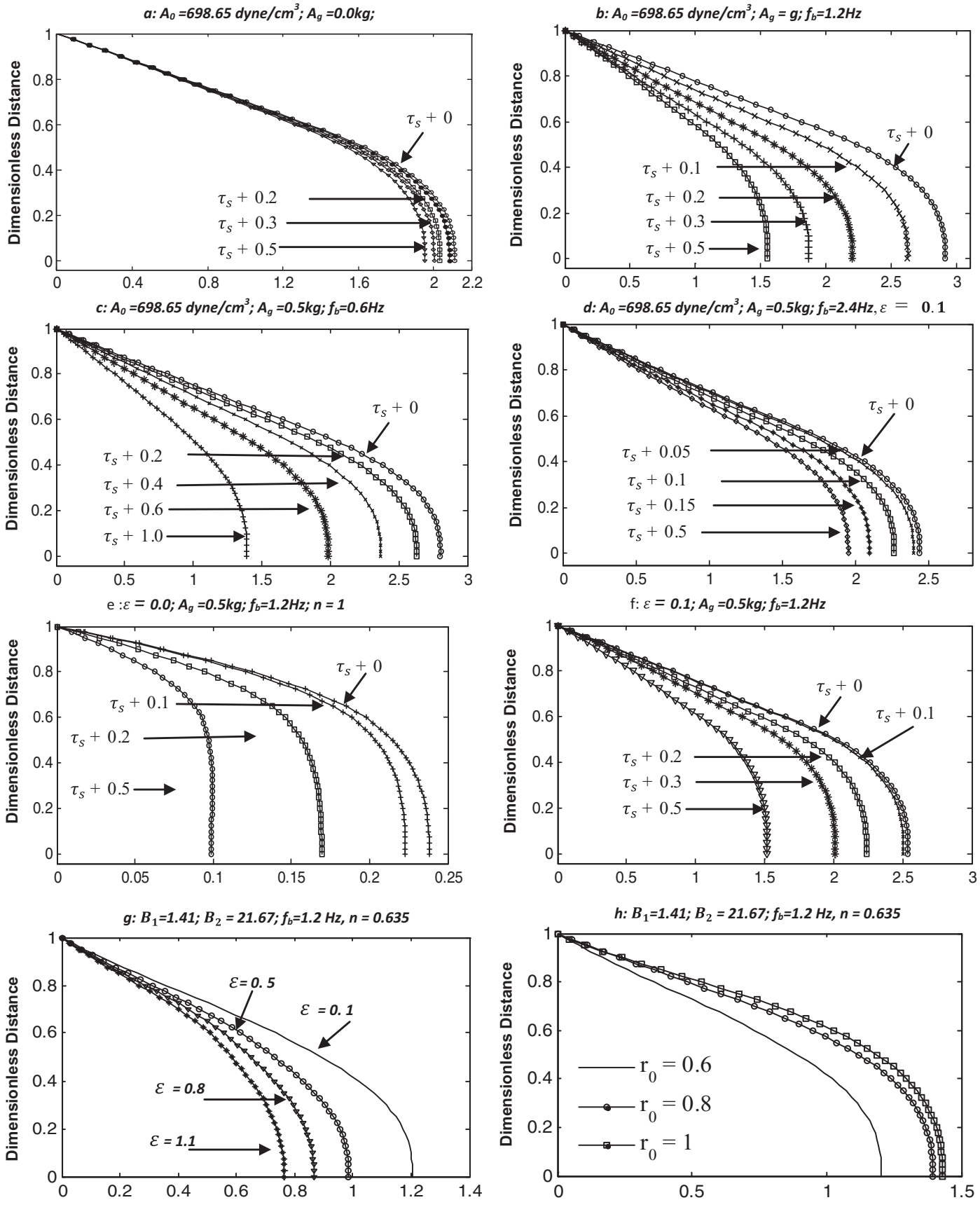


**Fig. 5.** Dimensionless velocity graphs for smaller artery (r = 0.15 cm, $A_0$ = 698.65 dyne/cm$^3$). The effects of $B_2$ (varying $A_g$) are shown in (a) and (b); velocity graphs for different values of $f_b$ are shown in (c) and (d); graphs for different values of $\varepsilon$ are shown in (e), (f) and (g); graphs for different peripheral thickness are shown in (h).

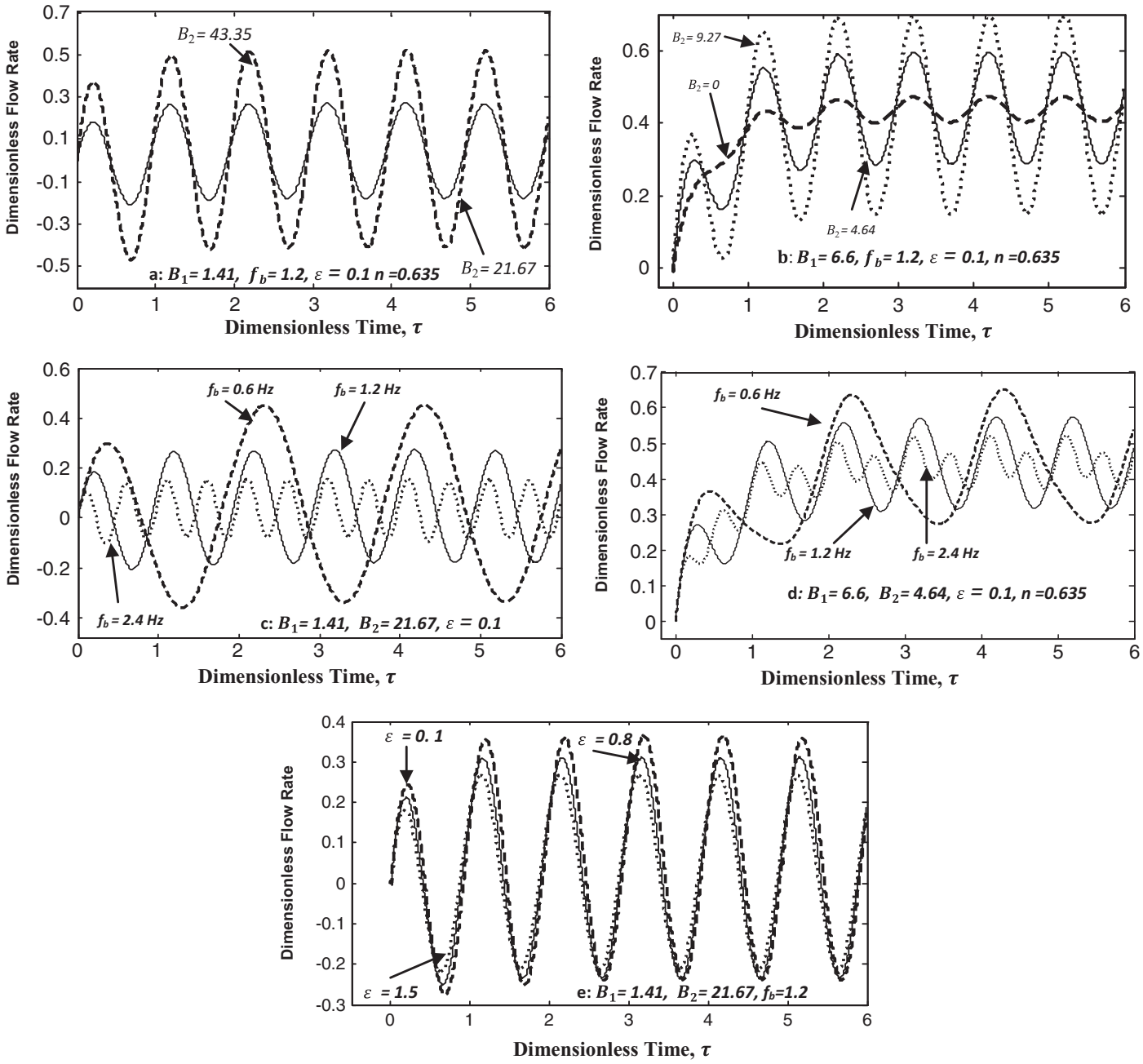


**Fig. 6.** Flow rate graphs in two different arteries for different values of emerging parameters. Flow rate for larger artery is shown in Fig. 6(a), (c) and (e) and in Fig. 6(b) and (d) for smaller artery. The effects of varying $B_2$ are shown in Fig. 6(a) and (b); graphs for different values of $f_b$ are shown in Fig. 6(c) and (d) and Fig. 5(e) shows the effects of varying $\varepsilon$.

constitutive equation of a Sisko model. The important phenomena associated with this equation are presented and discussed in detail with particular focus on interaction of these phenomena with pulsatile flow and body acceleration. The present analysis is more general and even such flow analysis with F-L effect in the Sisko fluid is not yet available in the literature. The following points are concluded from this study.

- The magnitude of blood velocity in the femoral artery is greater than in the coronary artery.
- Body acceleration increases the amplitude of the flow velocity.
- The material parameter of the Sisko model has greater influence on blood flow in coronary artery as compared to the femoral artery.
- This study also demonstrates the potential of rheological properties of the blood to control the important variables associated with the blood flow.
- The results obtained here show pleasing agreement with the existing results of Massoudi and Phuoc [20].

## Acknowledgments

The valuable suggestions of the anonymous reviewer are greatly appreciated. The first author, Akbar Zaman, is grateful to the HEC for financial assistance.

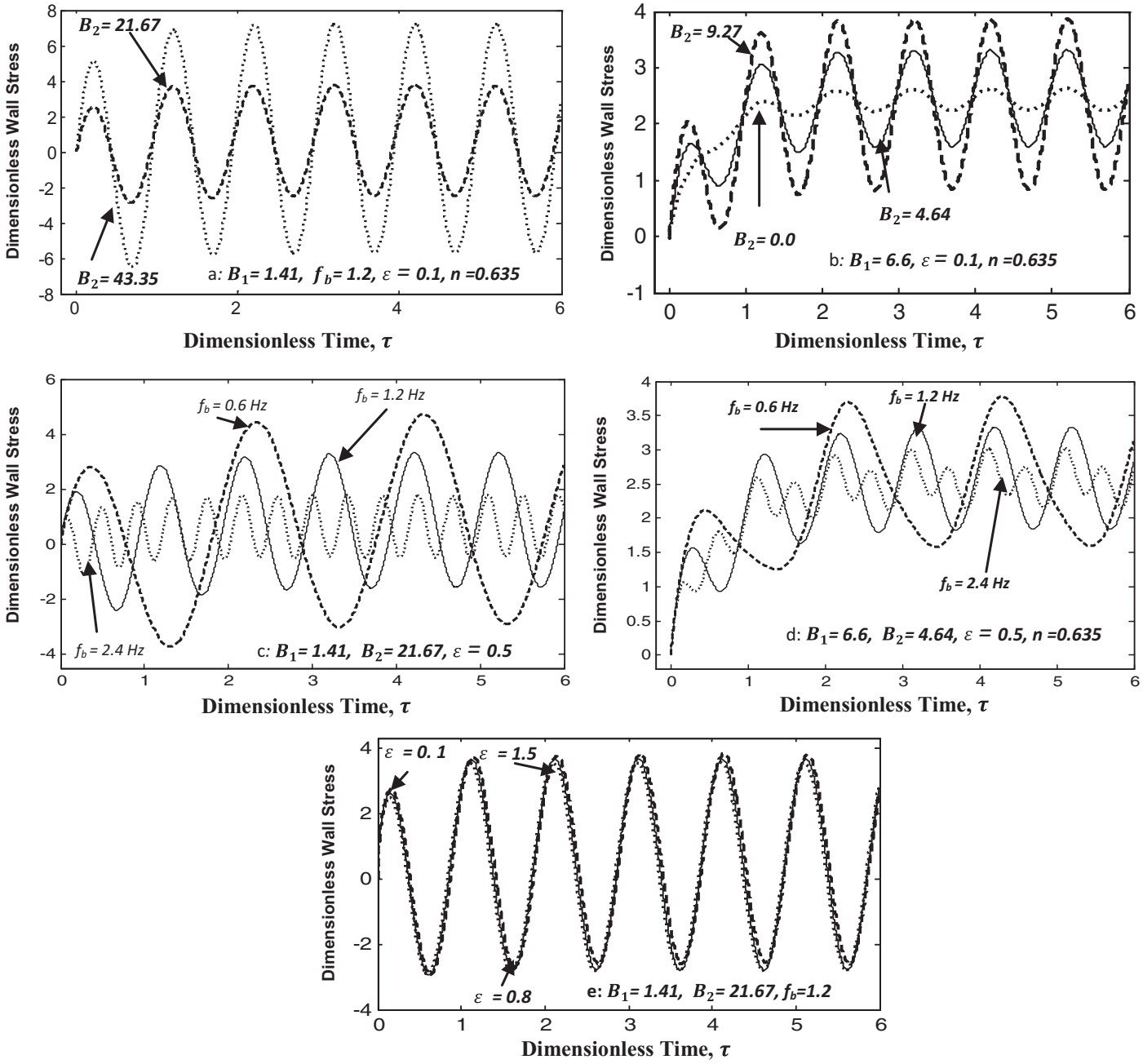


**Fig. 7.** Wall shear stress graphs in two different arteries for different values of emerging parameters. Wall shear stress for larger artery is shown in Fig. 7(a), (c) and (e) and in Fig. 7(b) and (d) for smaller artery. The effects of varying $B_2$ ($A_g = 0.5g$) are shown in Fig. 6(a) and (b); the effects of varying $f_b$ ($A_g = 0.5g$) are shown in Fig. 7(c) and (d) and Fig. 7(e) demonstrates the effects of varying $\varepsilon$.

## Nomenclature

| | |
|---|---|
| $a$ | Radius of core region |
| $A_0$ | Amplitude of the pressure gradient |
| $A_1$ | Amplitude of the pulsatile component |
| $A_g$ | Amplitude of the body acceleration |
| $b$ | Radius of an artery |
| $B_1$ | Dimensionless pulsatile constant |
| $B_2$ | Dimensionless body acceleration constant |
| $E$ | Ratio of the systolic to diastolic pressure |
| $f_p$ | Heart pulse frequency |
| $G(t)$ | Body acceleration |
| $N$ | Power law constant |
| $P$ | Pressure |
| $Q$ | Volumetric flow rate |
| $r$ | Radial co-ordinate |
| $T$ | Time |
| $u_1$ | Velocity component in core region |
| $u_2$ | Velocity component in periphery region |
| $U_0$ | Average velocity |

*Greek symbol*

| | |
|---|---|
| $\Pi$ | The second invariant of strain-rate tensor |
| $\boldsymbol{A}_1^*$ | first Rivlin–Ericksen tensor |
| $\mu_1$ | Viscosity of the non-Newtonian fluid |
| $\mu_2$ | Viscosity of the Newtonian fluid |

| | |
|---|---|
| $\rho_1$ | Density of the core fluid |
| $\rho_2$ | Density of the Plasma fluid |
| $\phi$ | Phase angle |
| $\omega_p$ | Circular frequency |
| $\varepsilon_1$ | Asymptotic value of viscosity at very high shear rates |
| $\varepsilon_2$ | Consistency |
| $\alpha$ | Womersley number of the non-Newtonian fluid |
| $\gamma$ | Womersley number of the Newtonian fluid |
| $\tau_s$ | Wall shear stress |
| $\mu^*$ | Dimensionless viscosity |
| $\rho^*$ | Dimensionless density |

## References


[1] F. Yilmaz, M.Y. Gundogdu, A critical review on blood flow in large arteries; relevance to blood rheology, viscosity models, and physiologic conditions, Korea Aust Rheol. J. 20 (2008) 197–211.
[2] R. Fahraeus, T. Lindqvist, The viscosity of blood in narrow capillary tubes, Am. J. Physiol. 96 (1931) 562–568.
[3] J.M. Lighthill, Physical fluid dynamics: a survey, J. Fluid Mech. 52 (1972) 475.
[4] G. Segre, A. Silberberg, Behavior of macroscopic rigid spheres in Poiseuille flow. Part 1, J. Fluid Mech. 14 (1962) 115–135.
[5] S.N. Majhi, L. Usha, Modeling the Fahraeus–Lindqvist effect through fluids of differential type, Int. J. Eng. Sci. 26 (1988) 503–508.
[6] S.N. Majhi, V.R. Nair, Pulsatile flow of third grade fluids under body acceleration – modeling blood flow, Int. J. Eng. Sci. 32 (1994) 839–846.
[7] K. Haldar, H.I. Andersson, Two-layered model of blood flow through stenosed arteries, Acta Mech. 117 (1996) 221–228.
[8] R. Usha, K. Prema, Pulsatile flow of a particle–fluid suspension model of blood under periodic body acceleration, Z. Angew. Math. Phys. ZAMP 50 (1999) 175–192.
[9] M. Anand, K.R. Rajagopal, A shear-thinning viscoelastic fluid model for describing the flow of blood, Int. J. Cardiovasc. Med. Sci. 4 (2004) 59–68.
[10] M. Anand, K.R. Rajagopal, A model for the formation and analysis of blood clots, Pathophysiol. Haemost. Thromb. 34 (2005) 109–120.
[11] J. Hron, J. Malek, S. Turek, A numerical investigation of flows of shear-thinning fluids with applications to blood rheology, Int. J. Numer. Methods Fluids 32 (2000) 863–879.
[12] G.B. Thurston, Viscoelasticity of human blood, Biophys. J. 12 (1979) 1205–1217.
[13] S. Chien, R.G. King, R. Skalak, S. Usami, A.L. Copley, Viscoelastic properties of human blood and red cell suspension, Biorheology 12 (1975) 341–346.
[14] J.C. Misra, B.K. Sahu, Flow through blood vessels under the action of a periodic acceleration field, Comput. Math. Appl. 16 (1988) 993–1016.
[15] M. El-Shahed, Pulsatile flow of blood through a stenosed porous medium under periodic body acceleration, Appl. Math. Comput. 138 (2003) 479–488.
[16] D.S. Sankar, K. Hemalatha, Pulsatile flow of Herschel–Bulkley fluid through stenosed arteries – a mathematical model, Int. J. Non Linear Mech. 41 (2006) 979–990.
[17] P. Chaturani, V. Palanisamy, Casson fluid model for pulsatile flow of blood under periodic body acceleration, Biorheology 27 (1990) 619–630.
[18] P. Chaturani, V. Palanisamy, Pulsatile flow of power-law fluid model for blood flow under periodic body acceleration, Biorheology 27 (1990) 747–758.
[19] P.K. Mandal, An unsteady analysis of non-Newtonian blood flow through tapered arteries with a stenosis, Int. J. Non Linear Mech. 40 (2005) 151–164.
[20] M. Massoudi, T.X. Phuoc, Pulsatile flow of a blood using second grade fluid model, Comput. Math. Appl. 56 (2008) 199–211.
[21] D.S. Sankar, Two-phase non-linear model for blood flow in asymmetric and axi-symmetric stenosed arteries, Int. J. Non Linear Mech. 46 (2011) 296–305.
[22] K.R. Madhura, B.J. Gireesha, C.S. Bagewadi, Exact solutions of unsteady dusty fluid flow through porous media in an open rectangular channel, Adv. Theor. Appl. Mech. 2 (2009) 1–17.
[23] B.J. Gireesha, C.S. Bagewadi, B.C. Prasannakumar, Pulsatile flow of an unsteady dusty fluid through rectangular channel, Commun. Nonlinear Sci. Numer. Simul. 14 (2009) 2103–2110.
[24] B.J. Gireesha, C.S. Bagewadi, B.C. Prasannakumara, Flow of unsteady dusty fluid under varying pulsatile pressure gradient in an holonomic co-ordinate system, Electron. J. Theor. Phys. 14 (2007) 9–16.
[25] H.A. Branes, J.F. Hutton, K. Walter, An Introduction to Rheology, Elsevier, Amsterdam, 1989.
[26] Y. Wang, T. Hayat, N. Ali, M. Oberlack, Magnetohydrodynamic peristaltic motion of a Sisko fluid in a symmetric or asymmetric channel, Physica A 387 (2008) 347–362.
[27] P. Chaturani, I.A.S. Wassf, Blood flow with body acceleration forces, Int. J. Eng. Sci. 33 (1995) 1807–1820.
[28] A.C. Burton, Physiology and Biophysics of the Circulation, Introductory Text, Year Book Medical Publisher, Chicago, 1966.
[29] P.K. Mandal, S. Chakravarty, A. Mandal, N. Amin, Effect of body acceleration on unsteady pulsatile flow of non-Newtonian fluid through a stenosed artery, Appl. Math. Comput. 189 (2007) 766–779.
[30] V.P. Rathod, M. Ravi, Blood flow through stenosed inclined tubes with periodic body acceleration in the presence of magnetic field and its applications to cardiovascular diseases, Int. J. Therm. Eng. 3 (1) (2014) 1–8.
[31] K.A. Hoffmann, S.T. Chiang, Computational Fluid Dynamics, vol. 1, Engineering Edition System, Wichita, KS, 2000.
[32] A. Zaman, N. Ali, M. Sajid, T. Hayat, Effects of unsteadiness and non-Newtonian rheology on blood flow through a tapered time-variant stenotic artery, AIP Adv. 5 (2015) 037129.